

Three-Dimensional to Layered Halide Perovskites: A Parameter-Free Hybrid Functional Method for Predicting Electronic Band Gaps

Ibrahim Buba Garba,[†] Lorenzo Trombini,[†] Claudine Katan,[†] Jacky Even,[‡] Marios Zacharias,[‡] Mikael Kepenekian,[†] and George Volonakis^{*,†}

[†]*Univ Rennes, ENSCR, CNRS, ISCR (Institut des Sciences Chimiques de Rennes), UMR 6226,
France*

[‡]*Univ Rennes, INSA Rennes, CNRS, Institut FOTON - UMR 6082, Rennes, France*

E-mail: yorgos.volonakis@univ-rennes.fr

Abstract

Accurately predicting electronic band gaps in halide perovskites using *ab initio* density functional theory (DFT) is essential for their application in optoelectronic devices. Standard hybrid functionals such as HSE and PBE0 can overcome the limitations of DFT with reasonable computational cost but are known to underestimate the measured band gaps for layered halide perovskites. In this study, we assess the performance of the doubly screened dielectric-dependent hybrid (DSH) functional for predicting band gaps in three-dimensional (3D) and layered hybrid perovskites. We show that the DSH functional, which employs material-dependent mixing parameters derived from macroscopic dielectric constants, provides accurate band gap predictions for 3D halide perovskites when structural local disorder is considered. For layered hybrid perovskites, we identified a challenge in setting the relevant screening parameter, and we found that the DSH functional based on average dielectric constants overestimates the band gaps. To improve the predictions and stay in a parameter-free *ab initio* workflow, we propose to use the calculated dielectric constant of the respective 3D perovskites. We find that the PBE0 and DSH functionals using the dielectric constants of the 3D perovskite accurately predict experimental gaps, with mean absolute errors of 0.21 eV and 0.14 eV, respectively, for layered perovskites with various organic spacers, as well as for multilayered $BA_2MA_{n-1}Pb_nI_{3n-1}$ with $n = 2, 3$. Notably, the HSE functional systematically underestimates the band gaps in layered perovskites, with absolute errors of 0.84 eV. We attribute the root of this failure to the absence of non-local long-range dielectric screening, a critical factor for halide perovskites. The computational framework introduced here provides an efficient parameter-free *ab initio* methodology for predicting the electronic properties of 3D and layered halide perovskites and their heterostructures, aiding in developing advanced optoelectronic devices.

Lead-based hybrid halide perovskites have emerged as versatile materials with tunable structural, electronic, and optical properties due to their unique inorganic corner-sharing octahedral lattices and complex organic components. These diverse material compositions enable a spectrum of functionalities that have been successfully applied in various technological fields, such as solar cells, photodetectors, and light-emitting devices.¹⁻⁴ Halide perovskites are generally classified into three-dimensional (3D) and layered halide perovskites. The 3D halide perovskites are represented by the general formula AMX_3 , where M is typically a divalent cation in the center of the octahedron such as Pb^{2+} or Sn^{2+} , X is a halogen (I, Br, or Cl), and the A site is typically occupied by Cs^+ or organic cations such as methylammonium (MA) or formamidinium (FA). In recent years, solar cells based on 3D halide perovskites have achieved remarkable power conversion efficiencies today comparable to those achieved by silicon cells.¹ However, these 3D materials can suffer from poor environmental stability when exposed to air and/or illumination.⁵ Their layered counterparts, also called two-dimensional (2D) halide perovskites, are further classified into Ruddlesden-Popper (RP), Dion-Jacobson (DJ), and alternating cation (ACI) structures, depending on the choice of organic molecules that separate the layers and the resulting stacking arrangement.⁶ For example, the RP structure typically has two monovalent organic cations and the general formula $A_2A'_{n-1}M_nX_{3n-1}$, where n is the number of connected MX_6 octahedra in the structure.⁷ Layered halide perovskites can exhibit significantly higher material stability than 3D perovskites. However, their photovoltaic performance is usually lower.^{8,9} Within these layered materials, the organic moieties are usually insulating; thus, the charge carriers are primarily constrained to the inorganic layers. This leads to the natural formation of quantum wells (QW), in which the optical band gap increases with decreasing n ($n = 1, 2, 3, \dots$) due to quantum and dielectric confinement.^{10,11} Most recently, the combination of the two in the so-called 3D/2D heterostructures has achieved superior stability compared to 3D and higher efficiency than layered halide perovskites, making them a promising platform for optimizing device performance in various architectures.¹² Consequently, knowledge about the energy levels is critical to monitor the band alignment between layered and 3D structures.¹²

Density Functional Theory (DFT) calculations, employing semi-local exchange-correlation (XC) functionals like the generalized gradient approximation (GGA) with spin-orbit coupling effects, lead to a sizable and systematic underestimation of the electronic band gap. The state-of-the-art method to go beyond DFT is Hedin's *GW* many-body quasiparticle perturbation theory¹³ that accounts for exchange-correlation effects via the self-energy, defined based on the Green's function, G , and the dynamical Coulomb screening potential W . The *GW* quasiparticle conduction band minimum (CBM) and valence band maximum (VBM) can be interpreted as the ionization energy (IE) measured by ultraviolet photoemission spectroscopy (UPS) and the electron affinity (EA) obtained from inverse photoemission spectroscopy (IPES), respectively. However, the *GW* approximation is computationally expensive,¹⁴ which limits its use in large systems containing hundreds or thousands of electrons, such as layered halide perovskites and very few works have reported the *GW* band gaps in the entire structure (i.e., including the organic moieties) of layered halide perovskites.^{15–19}

An alternative approach to *GW* is using the so-called hybrid functionals within DFT constructed by admixing a non-local Hartree fraction to the local exchange potential.²⁰ This mixing mitigates the self-interaction error, and has been shown for several semiconductors to result in improved band gaps and reasonable energy level alignment at a computational cost that can be significantly smaller than *GW* calculations.²¹ Well-known hybrid functionals include PBE0,²² which adds 25% (i.e., the mixing parameter α_H is set to 0.25) exact Hartree-Fock exchange to the exchange-correlation potential. HSE^{23,24} is similar to PBE0 but introduces a range-separation parameter μ that partition the Coulomb interaction into short- and long-range components. These hybrid functionals significantly improve standard DFT, yet PBE0 tends to overestimate band gaps, particularly for narrow band gap materials. At the same time, HSE underestimates band gaps of moderate band gap semiconductors and wide band insulators.²⁵ To overcome this limitation, the mixing parameters α_H and μ are often modified to reproduce experimental results, which limits the predictive capability of hybrid functionals.^{26–28} A good example of this limitation is the case of halide perovskites, for which hybrid functionals are being employed with a wide range of mixing

parameters, in many cases surpassing the 60% of exact exchange.²⁷⁻³⁰ Such manual tuning of the parameters in hybrid functionals is impractical and ineffective if the band gap of the material is not known *a priori*. It can also be challenging to predict suitable mixing parameters in complex heterostructures. Hence, it is desirable to develop mixing parameters independent of empirical tuning and have an intrinsic physical meaning.

To this end, it has been shown that the inverse macroscopic dielectric constant ϵ_{∞}^{-1} , which relates to the screening strength in materials, can be employed in a "parameter-free" dielectric-dependent hybrid functional (DDH) which gives good agreement with experiments for representative materials with a wide range of band gaps and dielectric constants.³¹⁻³³ A fully self-consistent version sc-DDH, which involves evaluating ϵ_{∞} at the end of each DDH cycle, was also developed.³⁴ A range-separated version (sc-RS-DDH),³⁵ with the long-range screening set at the empirical value of 0.25, has been proposed that further improves the band gap prediction with respect to sc-DDH. In the same spirit, but without any empirical parameter, two types of dielectric-dependent hybrid functionals have recently been introduced. First, the doubly screened dielectric-dependent hybrid (DSH) functional,³⁶ which accounts for both electronic and metallic screening, and the dielectric-dependent range-separated hybrid functional using the Coulomb attenuated method (DD-RS-CAM).³⁷ Although both functionals use the same model dielectric function,^{38,39} in each case the range separation parameter μ is determined slightly differently. In DSH, μ is derived from modified Thomas-Fermi screening, whereas in DD-RS-CAM μ is obtained by fitting the first-principles RPA dielectric function with the model dielectric function. Nevertheless, these two functionals are practically the same and do not give rise to significant differences in the predicted band gaps of materials.^{35,40} The model macroscopic dielectric function in DSH and DD-RS-CAM disregards both local field effects (i.e., off-diagonal elements) and dynamical effects and can be viewed as a static approximation to the diagonal Coulomb hole and screened exchange (COHSEX)^{13,41} approximation to the GW self-energy. Overall, the validity of this approximation depends on how well the semi-local correlation represents the Coulomb hole and the significance of the dynamical effects.³⁷ Table S1 summarizes the parameters of the different hybrid functionals.

To date, DSH has been applied to 3D halide perovskites,^{40,42–44} and, to the best of our knowledge, no reports are validating DSH for the prediction of the band gap of layered halide perovskites, which remains a challenge. Nevertheless, the computational studies on 3D perovskites employ high-symmetry structures and disregard effects arising from structural local disorder, which are critical for the description of halide perovskites, playing an important role on their structural, electronic, optical, and phonon properties.^{45–47} In this work, we compute the electronic band gaps of the most prominent 3D and layered halide perovskites using the DSH hybrid functional. We do so to explore the possibility of developing a consistent workflow that would permit calculating the band gaps of all these materials without having to tune any parameter of the hybrid functionals empirically. To this end, we consider a set of layered halide perovskites, known to pose a challenge for hybrid functionals, containing different organic cation spacers and different halogen atoms (i.e., Cl, Br, and I), as well as a layered perovskite series $BA_2(MA)_{n-1}Pb_nI_{3n+1}$ with $n = 2$ and $n=3$. All materials studied in this work are shown in Figure 1. We assess the performance of the DSH functional in both its one-shot (DSH0) and self-consistent (sc-DSH) forms, comparing the results with those obtained using typical hybrid functionals, such as HSE and PBE0, and experimental measurements. We also explore the importance of the hybrid functionals’ short- and long-range separation on band gap for each system.

We begin by analyzing how the doubly screened hybrid (DSH) functional performs on the prediction of the band gaps of prototypical cubic structures of 3D halide perovskites $CsPbX_3$ ($X = Cl, Br, I$). We model the structures using the lattice parameters that are summarized in Table S2. All computed band gaps include spin-orbit coupling effects, important in halide perovskites.⁴⁸ We compare these predictions with those obtained using PBE, PBE0, and HSE06, as well as the measured experimental electronic band gaps (See Table S2). Figure 2 shows the band gaps calculated employing different functionals (bars) and the measured band gaps (solid lines). As an additional reference, we include the standard semiconductors Si and GaAs, which have similar band gaps yet dielectric constants much higher than $CsPbX_3$. Not surprisingly, all hybrid functionals drastically improve the PBE band gap values. For the standard semiconductors, HSE values are very close to

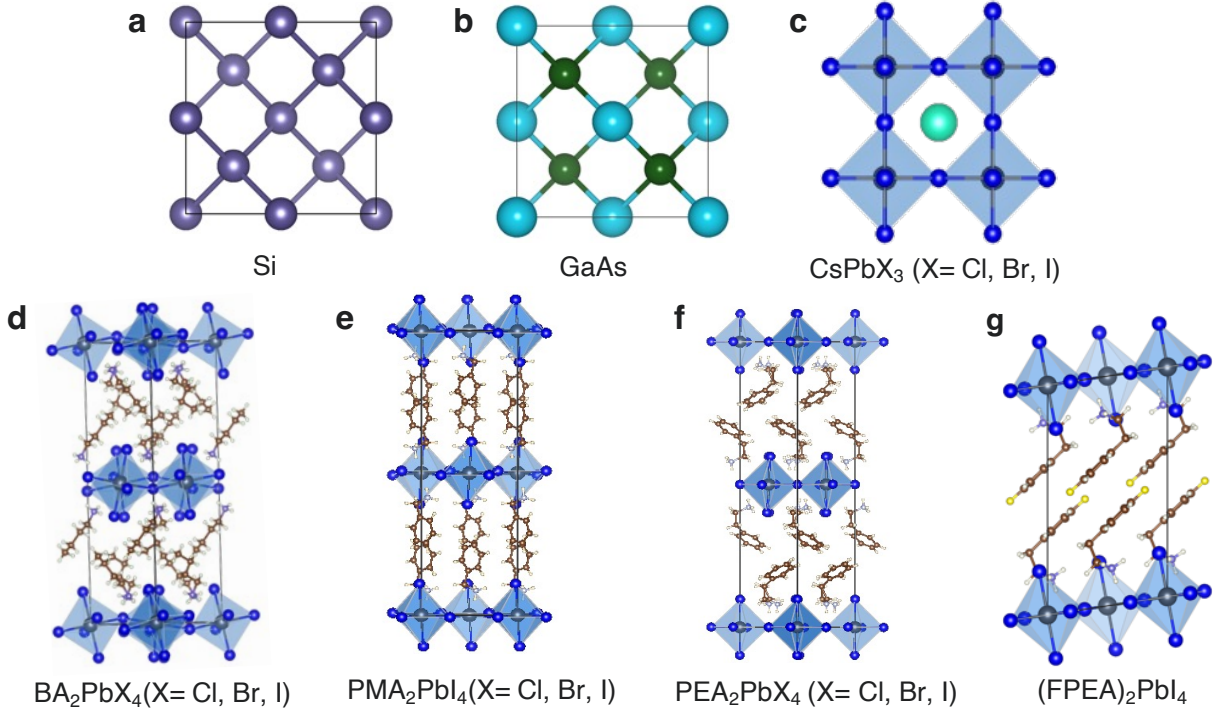


Figure 1: Polyhedral models of various materials with lattice parameters in Table S2 and S3: (a) Si; (b) GaAs; (c) 3D CsPbX_3 ($X = \text{Cl}, \text{Br}, \text{I}$) inorganic perovskites in the high-symmetry cubic phase; (d–g) 2D layered halide perovskites with different organic cations, including (d) BA_2PbX_4 , (e) PEA_2PbX_4 , (f) PMA_2PbX_4 , and (g) $\text{FPEA}_2\text{PbI}_4$.

the experimental band gaps, and so are the values obtained from the dielectric-dependent DSH0 and DSH. On the other hand, PBE0 significantly overestimates the band gap as range separation is critical for the functional form in both Si and GaAs. Moving on to the cubic phases of the 3D halide perovskites CsPbX_3 , the hybrid functionals fail to describe the band gaps as all functionals significantly underestimate the measured band gaps. However, this underestimation is related to neglecting local disorder (also referred to as positional "*polymorphism*"), which is critical for the accurate description of the electronic structure of halide perovskites at higher temperatures, including their dielectric properties.^{45–47,49} Some of us have previously shown that such local disorder (shown in the inset structures of Figure 2) has significant effects on the band gaps, lattice dynamics, and electron-phonon coupling of halide perovskites.^{46,47} Therefore, we consider the locally disordered configurations for CsPbX_3 (p- CsPbX_3) to assess the performance of the hybrid functionals. As shown in the last panel of Figure 2, we find a significant increase of the band gap values

resulting from the local disorder for all the functionals, ranging from 570 meV (PBE, p-CsPbCl₃) to 960 meV (DSH0, CsPbI₃), leading to a better agreement with the measurements.

For halide perovskites, the HSE functional underestimates the band gaps and underperforms with respect to PBE0. This important difference can be explained by looking into the details of the relationship between the screening and mixing of the parameters of functionals. HSE and PBE0 employ the same non-local short-range dielectric screening, but PBE0 includes 25% of long-range dielectric screening. This implies that for halide perovskites, the long-range dielectric screening needs to be close to the 25% or ϵ_{∞}^{-1} , like in the case of dielectric-dependent functionals. Furthermore, we note the relatively close band gap values between PBE0 and DSH for CsPbI₃. As the two functionals have comparable long-range dielectric screening effects ($\alpha_H = 0.25$ for PBE0 and 0.22 for DSH), yet very different short-range screening (0.25 for PBE0 and the full exact-exchange for DSH), range separation is not critical. The exact form of the screening for the materials is shown in Figure S1. When moving to lighter halogen atoms, the long-range dielectric screening fraction increases from 0.28 for p-CsPbBr₃ to 0.31 for p-CsPbCl₃, hence the DSH band gap values gradually diverge from PBE0. Overall, it is evident that for 3D halide perovskites, using the standard PBE0 or the DSH functional with polymorphous structures provides an efficient methodology for predicting band gaps without needing empirical tuning of the mixing fractions.

Next, we discuss the effects of self-consistency on improving DSH band gaps. In both full-range³⁴ and range-separated dielectric dependent hybrid functionals,^{36,37} early results indicated that self-consistency improves the band gaps values compared to one-shot methods, especially for narrow band gap materials.³⁶ However, such self-consistency worsens the results for transition metal oxides, which is attributed to the underestimated dielectric constants.⁵⁰ Here, we observe that self-consistency leads to relatively minor changes in the calculated band gaps, with the change being marginal in the case of Si, GaAs, and p-CsPbI₃. Figure S3 shows the band gap variation and dielectric constants for each DSH iteration. We also note that the method employed to evaluate ϵ_{∞} in the self-consistency cycle can be critical. ϵ_{∞} can be computed using different methods, including density functional perturbation theory (DFPT),⁵¹ finite electric field in the Berry phase

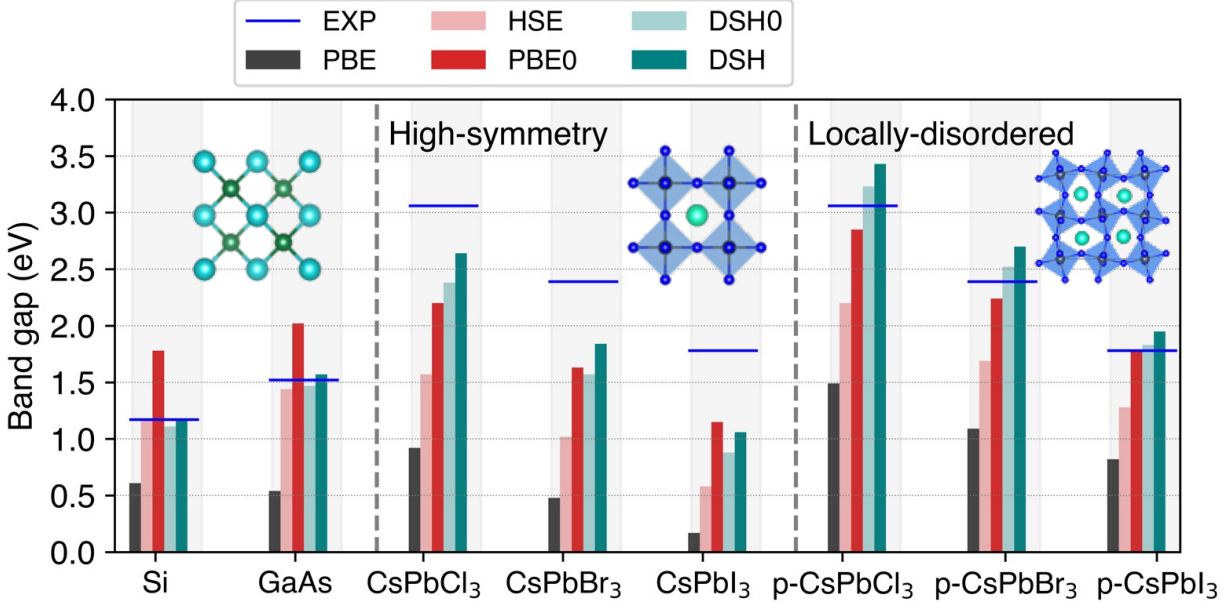


Figure 2: Band gaps of three-dimensional bulk semiconductors calculated using PBE (black), HSE (salmon), PBE0 (red), DSH0 (light green), and DSH (dark green). The electronic experimental band gaps are represented by the blue horizontal line (See Table S2 for values). The significant enhancement of the band gap observed in p-CsPbX₃ across all the functionals is primarily due to structural local disorder within the material.

approximation,⁵² or linear optics in the Random Phase Approximation (RPA),⁵³ each with different advantages and limitations discussed in the supporting information file. Here, we employ the finite electric field method, as detailed in the computational details, to include local field effects, which are important for halide perovskites. However, converging ϵ_{∞} remains challenging when employing hybrid functionals.

Next, we employ the DSH functional to set up a parameter-free workflow for layered halide perovskite materials. To this end, we consider a series of prototypical lead-based layered structures with various halogen atoms (i.e., Cl, Br, I) and different organic spacers, as seen in Table S3. Figure 1d-g shows the materials with the organic cations BA (butylammonium), PMA (phenylmethyl ammonium), PEA (phenylethylammonium) and FPEA (4F-phenylethylammonium), respectively. We have not considered locally disordered structures for the layered perovskites, as our calculations are based on experimental low-symmetry structures with significant distortion and therefore, the effects are expected to be small. For example, the change in total energy due to structural

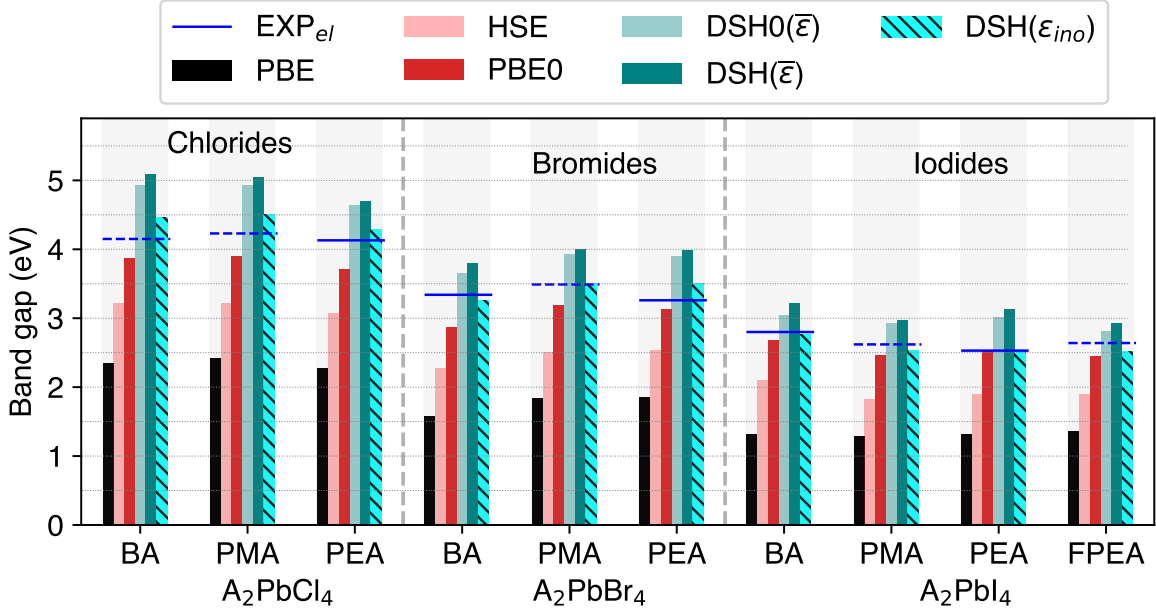


Figure 3: Comparison of band gaps in layered halide perovskites using PBE (grey), HSE (salmon), PBE0 (red), DSH0 (light-green), DSH($\bar{\epsilon}$) (dark-green) and DSH(ϵ_{ino}) (hatched turquoise). The electronic experimental band gap values (EXP_{el}) (see Table S3), are indicated by the blue horizontal lines, and dotted blue lines are derived by adjusting the optical gaps E_g^{op} , with exciton binding energy E_b , where $E_b = 0.18E_g^{el} - 0.249$.⁵⁴

local disorder for orthorhombic CsPbI₃ is reported at just 1 meV per formula unit.⁴⁶ Also, in the absence of experimental electronic band gaps, we correct the experimental optical band gaps (E_g^{op}) using the empirical relation of the exciton binding energy (E_b), derived for layered perovskites (i.e., $E_b = 0.18E_g^{el} - 0.249$).⁵⁴ The *ab initio* computation of the exciton binding energy would require to solve the GW plus Bethe-Salpeter equation (GW+BSE). To date, only a handful of studies have used the GW+BSE method to compute band gap and exciton binding energy in the full structure (i.e., including organic moieties) of layered halide perovskites.^{15–19} For example, Yin et al.¹⁵ investigated the origin of light emission in two layered perovskites. Giorgi et al.¹⁶ calculated the optoelectronic properties of isolated and layered $BA_2(MA)_{n-1}Pb_nI_{3n+1}$ with $n=1$ and $n=2$. Filip et al.¹⁸ analyzed the effects of various organic cations on the band gaps, dielectric screening, and exciton binding energies of a set of A_2PbBr_4 compounds.

For the DSH band gap calculation, assigning a single value to the dielectric screening (ϵ_∞^{-1})

for any layered perovskite is particularly challenging as the materials are composed of layers of moieties (i.e., organic and inorganic) with different dielectric constants, hence are not homogeneous. The first, most trivial option is to use the average of the main components of the dielectric tensor (i.e., the average of the diagonal) to define the Hartree exact exchange fraction, that is $\alpha_H = (\bar{\epsilon})^{-1}$ with $\bar{\epsilon} = (\epsilon_{xx} + \epsilon_{yy} + \epsilon_{zz})/3$. The calculated band gaps within the one-shot DSH0($\bar{\epsilon}$) and self-consistent DSH($\bar{\epsilon}$) method for layered perovskites are shown in Figure 3. Similar to 3D CsPbX₃, the band gaps calculated employing the PBE and HSE functionals are largely underestimated compared to experiment. The band gap increases from PBE to HSE, PBE0, DSH0($\bar{\epsilon}$) and finally DSH($\bar{\epsilon}$). However, we find that both DSH0($\bar{\epsilon}$) and DSH($\bar{\epsilon}$) functionals overestimate the band gaps across all the layered materials irrespective of the crystal symmetry, organic cation, or the type of halogen in the perovskite layer. Taking for example BA₂PbBr₄ (room temperature phase), DSH0($\bar{\epsilon}$) predicts a band gap of 3.65 eV, which is 0.31 eV higher than the experimental value of 3.34 eV reported by Silver et al.⁵⁵ The self-consistent DSH method, DSH($\bar{\epsilon}$), yields an even higher value of 3.79 eV, exceeding the experimental result by 0.45 eV. This trend is consistent across all layered materials studied here and can be explained as the screening for the DSH0 and DSH is based on $\bar{\epsilon}$, which includes contributions from the inorganic perovskite and the organic layer. In other words, the dielectric screening is an average of a low dielectric constant of the organic layer and a higher one of the inorganic layer. However, for the layered halide perovskites of interest here, the electronic band edges that define the electronic band gap are composed of states of the inorganic layer, as the valence band is mainly Pb 6*s*-orbitals and the halogen atoms *p*-orbitals, while the conduction band minimum is mostly of Pb 6*p*-orbitals and the halogens *p* orbitals.^{56,57} Therefore, one can argue that using DSH with the dielectric constant solely of the inorganic perovskite layer is more reasonable for predicting the band gaps accurately.

Considering the cubic phases of 3D halide perovskites allows defining unambiguously ϵ_∞ . Yet, for layered halide perovskites there are various methods developed to extract the dielectric constants of the inorganic (ϵ_{ino}) and organic (ϵ_{org}) layers. For example, ϵ_{ino} can be approximated as the bulk dielectric constant of the respective halide salt PbI₂.⁵⁸ One can employ a dielectric

profile calculated using different flavors of DFT to assess ϵ_{ino} and ϵ_{org} ,^{59,60} or model the structure using a two capacitor model and fit the dielectric constants along one⁵⁴ or both directions.⁶¹ While these methods can provide reasonable estimates of the dielectric constants, the challenge remains in accurately defining the model’s parameters, for example, the thickness of the inorganic layers or defining a clean interface between the two layers. Moreover, the accuracy of the dielectric constant depends on the choice of the DFT functional; the semi-local PBE functional, for example, tends to overestimate dielectric constants and gives divergent values for materials with narrow band gaps.³⁶ To overcome this issue in a simple way that is easy to implement in an *ab initio* parameter-free workflow, we propose employing the DSH using the dielectric constant of the 3D polymorphous perovskites to set the screening parameter. This method corresponds to the band gaps denoted as $\text{DSH}(\epsilon_{\text{ino}})$ shown in Figure 3 and summarized in Table S3. The band gap values predicted within $\text{DSH}(\epsilon_{\text{ino}})$ is a significant improvement with respect to the other functionals. For example, the band gap of BA_2PbBr_4 using $\text{DSH}(\epsilon_{\text{ino}})$ is 3.26 eV, in excellent agreement with the experimental value of 3.34 eV.⁵⁵ Interestingly, PBE0 also gives band gaps close to the measured electronic band gaps and similar to $\text{DSH}(\epsilon_{\text{ino}})$. For the iodides in particular, the similar performance of PBE0 and $\text{DSH}(\epsilon_{\text{ino}})$ can be attributed to a similar Hartree fraction for the long-range screening, which is $\alpha_H = 0.25$ in PBE0, and $\alpha_H = 0.22$ in $\text{DSH}(\epsilon_{\text{ino}})$ as ϵ_{ino} is 4.52, and the effects from the short-range screening is less important as the case of 3D halide perovskites shown in Figure 2. Similarly, for bromides, $\text{DSH}(\epsilon_{\text{ino}})$ is slightly above the measured band gaps, and PBE0 slightly below, which can also be attributed to the different screening at the long-range as $\epsilon_{\text{ino}} = 3.59$, yields α_H of 0.28. In contrast, for chlorides an $\epsilon_{\text{ino}} = 3.2$ gives an α_H of 0.31. The exact shape of the screening for all layered perovskites studied here is shown in Figure S2.

In order to quantify the performance of the different functionals in describing the band gap of layered halide perovskites, we calculate the mean absolute error (MAE) and root mean square error (RMSE). Figure 4a summarizes the performance of all hybrid functionals for all the layered materials, as well as by halogen (A_2PbCl_4 , A_2PbBr_4 , A_2PbI_4). The HSE functional is the least suitable, with errors close to 1.0 eV. PBE0, on the other hand, predicts the band gap reasonably

well across the layered materials, particularly for iodides. The proposed DSH0(ϵ_{ino}) has a similar performance and gives the most minor errors overall for bromides and iodides. In particular, the MAE and RMSE are below 80 meV for iodine-based materials. We also include two Dion-Jacobson layered halide perovskites (see Table S3), further validating the observed performance trend for all layered materials. Since in DSH(ϵ_{ino}), a fixed Hartree fraction is adopted to set the screening in layered perovskites with the same halogen. Consequently, any variation of the band gap of materials with the same inorganic layer can be attributed to structural distortions of the PbX_6 octahedra due to the different organic cations. For instance, $\text{PEA}_2\text{PbBr}_4$ and $\text{PMA}_2\text{PbBr}_4$ have similar Pb-X-Pb bond angles of 151° and 150° respectively, resulting in practically identical band gaps of 3.50 eV. While BA_2PbBr_4 , which exhibits slightly less octahedral distortion with the Pb-X-Pb angle amounting to 155° , the band gap is narrower 3.26 eV as the orbital overlap increases. A similar trend also applies to the iodides. This relationship between the increase in Pb-X-Pb distortion with the increase in the band gap is well documented and understood both theoretically³ and experimentally.⁶²

Finally, since the DSH(ϵ_{ino}) is successfully predicting the band gaps of both 3D and the different types of layered halide perovskites, we extend our analysis to verify that this approach can also predict band gaps for layered materials with a thicker inorganic layer (i.e., larger n -numbers). Thus, we apply our method to $\text{BA}_2(\text{MA})_{n-1}\text{Pb}_n\text{I}_{3n+1}$, where n is the number of octahedrons in the inorganic layer. We find that the band gap decreases as n increases, which is expected due to the reduction of the quantum, and dielectric confinement.^{3,10,65} We also note that to avoid introducing an artificial dipole due to the specific orientation of the organic molecule in the perovskite lattice, for $n = 2$ and $n = 3$, we replace MA in $\text{BA}_2(\text{MA})_{n-1}\text{Pb}_n\text{I}_{3n+1}$ with Cs (see the inset of Figure 4). The calculated band gaps employing PBE0 and DSH(ϵ_{ino}) are compared to experimental electronic band gaps shown in Figure 4. For the 3D case, we employ the DSH experimental band gaps of p-CsPbI₃. As shown in Figure 4, the DSH(ϵ_{ino}) band gaps agree well with the experiments for the complete series of $n = 1, 2, 3$. Notably, our band gap for $n = 1$ is comparable to the GW band gap reported by Giorgi et al.¹⁶ and the experimental values reported in Table S4. This comparison also

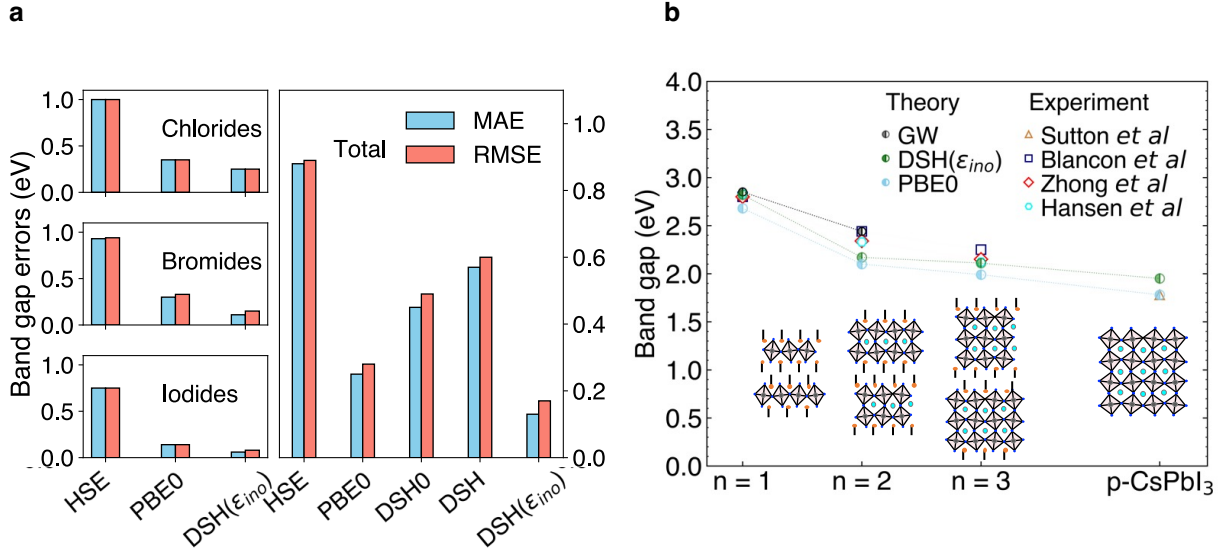


Figure 4: (a) Comparison of Mean Absolute Error (MAE) and Root Mean Square Error (RMSE) of HSE, PBE0, DSH0($\bar{\epsilon}$), DSH($\bar{\epsilon}$), and DSH(ϵ_{ino}) functionals with respect to experimental electronic band gaps of 2D layered halide perovskites grouped by the same halogen in left and total in right. (b) Electronic band gaps of the layered $BA_2(MA)_{n-1}Pb_nI_{3n+1}$ series ($n = 1, 2, 3$) and 3D (p-CsPbI₃), computed using PBE0 (sky-blue circles) and DSH(ϵ_{ino}) (green circles) compared with GW calculation¹⁶ (black circles) and experimental values from Blancon *et al.*,¹⁰ Zhong *et al.*,⁶³ Hansen *et al.*⁵⁴ for $n = 1, 2, 3$, and *et al.*⁶⁴ for the 3D case (See Table S4)

highlights the predictive accuracy of DSH(ϵ_{ino}). It offers a useful framework that can be used for other layered halide perovskites and their heterostructures with other 3D materials.

Overall, we present results for the band gaps of 3D and layered halide perovskite materials employing a consistent workflow to optimally set up the doubly screened dielectric-dependent hybrid (DSH) functional. Our results demonstrate that the proposed DSH(ϵ_{ino}) functional, which incorporates only material-dependent mixing parameters like the macroscopic high-frequency dielectric constants, predicts the band gaps with better accuracy than standard hybrid functionals in both 3D and layered perovskites. Our findings underline the importance of accounting for local disorder when benchmarking any functional for 3D halide perovskites. For the layered materials, it is evident that special attention needs to be taken when setting the screening based on the macroscopic dielectric function, for example, DSH0($\bar{\epsilon}$) and DSH($\bar{\epsilon}$), using the average of the diagonal components of the dielectric constant matrix tend to overestimate the measure band gaps. However, we used the DSH functional with the dielectric constants of the corresponding 3D perovskites,

DSH(ϵ_{ino}), described at room-temperature with polymorphous structures, to predict band gaps. We achieve remarkable performance in predicting experimental electronic band gaps across all the layered perovskites considered, irrespective of the type of organic spacer, especially for iodine-based materials. We observe that for all the materials (i.e., 3D and layered), the HSE functional significantly and systematically underestimates the band gaps due to the absence of non-local long-range dielectric screening. On the other hand, the PBE0 functional that shares the same non-local short-range screening with HSE but has an additional 25% non-local long-range screening performs very well. It could be the functional of choice if one cannot afford to compute the dielectric properties of halide perovskites. The computational strategy presented here sets up a parameter-free *ab initio* methodology that allows efficient prediction of the electronic properties of both 3D and layered halide perovskites. As such, the proposed workflow and benchmark can be extremely powerful in investigating 3D/2D heterostructures, which are challenging to describe at the *ab initio* level, while being attractive to develop stable and efficient opto-electronic devices.

Acknowledgement

I.B.G acknowledges discussions with Cui Zhi-Hao on the implementation of DSH functional in the VASP code. G.V. and I.B.G. acknowledge funding from the Agence Nationale pour la Recherche through the CPJ program and the SURFIN project (ANR-23-CE09-0001). This work was granted access to the HPC resources of TGCC under the Allocation Grant No. 2022 - A0130907682 made by GENCI and Lumi. M.Z. was funded by the European Union (project ULTRA-2DPK / HORIZON-MSCA-2022-PF-01 / Grant Agreement No. 101106654). Views and opinions expressed are however those of the authors only and do not necessarily reflect those of the European Union or the European Commission. Neither the European Union nor the granting authority can be held responsible for them. We acknowledge computational resources from the EuroHPC Joint Undertaking and supercomputer LUMI [<https://lumi-supercomputer.eu/>], hosted by CSC (Finland) and the LUMI consortium through a EuroHPC Extreme Scale Access call.

Supporting Information Available

Doubly screened dielectric dependent hybrid functional; Computational details; Comparison of model dielectric functions in hybrid functionals; Lattice constants and band gaps of 3D perovskites calculated using different functionals in Figure 2; Band gaps of layered halide perovskites calculated using different functionals in Figure 3; Band gaps of BA series in Figure 4; Comparison of model dielectric functions for hybrid functionals in 3D perovskites; Comparison of model dielectric functions for hybrid functionals in layered halide perovskites; Convergence of dielectric constant and band gap with self-consistent DSH iteration in 3D perovskites

References

- (1) Peng, W.; Mao, K.; Cai, F.; Meng, H.; Zhu, Z.; Li, T.; Yuan, S.; Xu, Z.; Feng, X.; Xu, J. et al. Reducing Nonradiative Recombination in Perovskite Solar Cells with a Porous Insulator Contact. *Science* **2023**, *379*, 683–690.
- (2) Li, X.; Hoffman, J. M.; Kanatzidis, M. G. The 2D Halide Perovskite Rulebook: How the Spacer Influences Everything from the Structure to Optoelectronic Device Efficiency. *Chem. Rev.* **2021**, *121*, 2230–2291.
- (3) Katan, C.; Mercier, N.; Even, J. Quantum and Dielectric Confinement Effects in Lower-Dimensional Hybrid Perovskite Semiconductors. *Chem. Rev.* **2019**, *119*, 3140–3192.
- (4) Han, T.-H.; Jang, K. Y.; Dong, Y.; Friend, R. H.; Sargent, E. H.; Lee, T.-W. A Roadmap for the Commercialization of Perovskite Light Emitters. *Nat. Rev. Mater.* **2022**, *7*, 757–777.
- (5) An, Y.; Hidalgo, J.; Perini, C. A. R.; Castro-Méndez, A.-F.; Vagott, J. N.; Bairley, K.; Wang, S.; Li, X.; Correa-Baena, J.-P. Structural Stability of Formamidinium- and Cesium-Based Halide Perovskites. *ACS Energy Lett.* **2021**, *6*, 1942–1969.
- (6) Blancon, J.-C.; Even, J.; Stoumpos, C. C.; Kanatzidis, M. G.; Mohite, A. D. Semiconductor Physics of Organic-Inorganic 2D Halide Perovskites. *Nat. Nanotechnol.* **2020**, *15*, 969–985.
- (7) Mitzi, D. B.; Wang, S.; Feild, C. A.; Chess, C. A.; Guloy, A. M. Conducting Layered Organic-inorganic Halides Containing $\langle 110 \rangle$ -Oriented Perovskite Sheets. *Science* **1995**, *267*, 1473–1476.
- (8) Li, W.; Sidhik, S.; Traore, B.; Asadpour, R.; Hou, J.; Zhang, H.; Fehr, A.; Essman, J.; Wang, Y.; Hoffman, J. M. et al. Light-activated interlayer contraction in two-dimensional perovskites for high-efficiency solar cells. *Nat. Nanotechnol.* **2022**, *17*, 45–52.
- (9) Cucco, B.; Leveillee, J.; Ha, V.-A.; Even, J.; Kepenekian, M.; Giustino, F.; Volonakis, G.

- Intrinsic Limits of Charge Carrier Mobilities in Layered Halide Perovskites. *PRX Energy* **2024**, *3*, 023012.
- (10) Blancon, J.-C.; Stier, A. V.; Tsai, H.; Nie, W.; Stoumpos, C. C.; Traoré, B.; Pedesseau, L.; Kepenekian, M.; Katsutani, F.; Noe, G. T. et al. Scaling Law for Excitons in 2D Perovskite Quantum Wells. *Nat. Commun.* **2018**, *9*, 2254.
- (11) Gedda, M.; Yengel, E.; Faber, H.; Paulus, F.; Kreß, J. A.; Tang, M.-C.; Zhang, S.; Hacker, C. A.; Kumar, P.; Naphade, D. R. et al. Ruddlesden–Popper-Phase Hybrid Halide Perovskite/Small-Molecule Organic Blend Memory Transistors. *Adv. Mater.* **2021**, *33*, 2003137.
- (12) Metcalf, I.; Sidhik, S.; Zhang, H.; Agrawal, A.; Persaud, J.; Hou, J.; Even, J.; Mohite, A. D. Synergy of 3D and 2D Perovskites for Durable, Efficient Solar Cells and Beyond. *Chem. Rev.* **2023**, *123*, 9565–9652.
- (13) Hedin, L. New Method for Calculating the One-Particle Green’s Function with Application to the Electron-Gas Problem. *Phys. Rev.* **1965**, *139*, A796–A823.
- (14) Umari, P.; Mosconi, E.; De Angelis, F. Relativistic GW calculations on CH₃NH₃PbI₃ and CH₃NH₃SnI₃ Perovskites for Solar Cell Applications. *Scientific Reports* **2014**, *4*.
- (15) Yin, J.; Li, H.; Cortecchia, D.; Soci, C.; Brédas, J.-L. Excitonic and Polaronic Properties of 2D Hybrid Organic–Inorganic Perovskites. *ACS Energy Lett.* **2017**, *2*, 417–423.
- (16) Giorgi, G.; Yamashita, K.; Palummo, M. Nature of the Electronic and Optical Excitations of Ruddlesden–Popper Hybrid Organic–Inorganic Perovskites: The Role of the Many-Body Interactions. *J. Phys. Chem. Lett.* **2018**, *9*, 5891–5896.
- (17) Molina-Sánchez, A. Excitonic States in Semiconducting Two-Dimensional Perovskites. *ACS Appl. Energy Mater.* **2018**, *1*, 6361–6367.

- (18) Filip, M. R.; Qiu, D. Y.; Del Ben, M.; Neaton, J. B. Screening of Excitons by Organic Cations in Quasi-Two-Dimensional Organic–Inorganic Lead-Halide Perovskites. *Nano Lett.* **2022**, *22*, 4870–4878.
- (19) Leppert, L. Excitons in Metal-halide Perovskites from First-principles Many-body Perturbation Theory. *J. Chem. Phys.* **2024**, *160*, 050902.
- (20) Martin, R. M. *Electronic structure: basic theory and practical methods*; Cambridge university press, 2020.
- (21) Chen, W.; Pasquarello, A. Band-edge Positions in *GW*: Effects of Starting Point and Self-consistency. *Phys. Rev. B* **2014**, *90*, 165133.
- (22) Perdew, J. P.; Ernzerhof, M.; Burke, K. Rationale for Mixing Exact Exchange with Density Functional Approximations. *J. Chem. Phys.* **1996**, *105*, 9982–9985.
- (23) Heyd, J.; Scuseria, G. E.; Ernzerhof, M. Hybrid Functionals Based on a Screened Coulomb Potential. *J. Chem. Phys.* **2003**, *118*, 8207–8215.
- (24) Krukau, A. V.; Vydrov, O. A.; Izmaylov, A. F.; Scuseria, G. E. Influence of the Exchange Screening Parameter on the Performance of Screened Hybrid Functionals. *J. Chem. Phys.* **2006**, *125*, 224106.
- (25) Steiner, K.; Chen, W.; Pasquarello, A. Band Offsets of Lattice-matched Semiconductor Heterojunctions Through Hybrid Functionals and G_0W_0 . *Phys. Rev. B* **2014**, *89*, 205309.
- (26) He, J.; Franchini, C. Screened Hybrid Functional Applied to $3d^0 \rightarrow 3d^8$ Transition-metal Perovskites LaMO_3 ($M = \text{Sc–Cu}$): Influence of the Exchange Mixing Parameter on the Structural, Electronic, and Magnetic properties. *Phys. Rev. B* **2012**, *86*, 235117.
- (27) Du, M.-H. Efficient Carrier Transport in Halide Perovskites: Theoretical Perspectives. *J. Mater. Chem. A* **2014**, *2*, 9091–9098.

- (28) Traore, B.; Even, J.; Pedesseau, L.; Képeñekian, M.; Katan, C. Band gap, effective masses, and energy level alignment of 2D and 3D halide perovskites and heterostructures using DFT-1/2. *Phys. Rev. Mater.* **2022**, *6*, 014604.
- (29) Basera, P.; Singh, A.; Gill, D.; Bhattacharya, S. Capturing Excitonic and Polaronic Effects in Lead Iodide Perovskites Using Many-body Perturbation Theory. *J. Mater. Chem. C* **2021**, *9*, 17113–17123.
- (30) Li, X.; Fu, Y.; Pedesseau, L.; Guo, P.; Cuthriell, S.; Hadar, I.; Even, J.; Katan, C.; Stoumpos, C. C.; Schaller, R. D. et al. Negative Pressure Engineering with Large Cage Cations in 2D Halide Perovskites Causes Lattice Softening. *J. Am. Chem. Soc.* **2020**, *142*, 11486–11496.
- (31) Alkauskas, A.; Broqvist, P.; Pasquarello, A. Defect levels Through Hybrid Density Functionals: Insights and applications. *Phys. Status Solidi B* **2011**, *248*, 775–789.
- (32) Marques, M. A. L.; Vidal, J.; Oliveira, M. J. T.; Reining, L.; Botti, S. Density-based Mixing Parameter for Hybrid Functionals. *Phys. Rev. B* **2011**, *83*, 035119.
- (33) Moussa, J. E.; Schultz, P. A.; Chelikowsky, J. R. Analysis of the Heyd-Scuseria-Ernzerhof density functional parameter space. *J. Chem. Phys.* **2012**, *136*, 204117.
- (34) Skone, J. H.; Govoni, M.; Galli, G. Self-consistent Hybrid Functional for Condensed Systems. *Phys. Rev. B* **2014**, *89*, 195112.
- (35) Skone, J. H.; Govoni, M.; Galli, G. Nonempirical Range-separated Hybrid Functionals for Solids and molecules. *Phys. Rev. B* **2016**, *93*, 235106.
- (36) Cui, Z.-H.; Wang, Y.-C.; Zhang, M.-Y.; Xu, X.; Jiang, H. Doubly Screened Hybrid Functional: An Accurate First-Principles Approach for Both Narrow- and Wide-Gap Semiconductors. *J. Phys. Chem. Lett.* **2018**, *9*, 2338–2345.

- (37) Chen, W.; Miceli, G.; Rignanese, G.-M.; Pasquarello, A. Nonempirical Dielectric-dependent Hybrid Functional with range separation for Semiconductors and Insulators. *Phys. Rev. Mater.* **2018**, *2*, 073803.
- (38) Cappellini, G.; Del Sole, R.; Reining, L.; Bechstedt, F. Model Dielectric Function for Semiconductors. *Phys. Rev. B* **1993**, *47*, 9892–9895.
- (39) Shimazaki, T.; Asai, Y. Band Structure Calculations Based on Screened Fock Exchange Method. *Chem. Phys. Lett.* **2008**, *466*, 91–94.
- (40) Yang, J.; Falletta, S.; Pasquarello, A. Range-separated Hybrid functionals for Accurate Prediction of Band Gaps of Extended Systems. *npj Comput. Mater.* **2023**, *9*.
- (41) Gygi, F.; Baldereschi, A. Quasiparticle Energies in Semiconductors: Self-energy Correction to the Local-density Approximation. *Phys. Rev. Lett.* **1989**, *62*, 2160–2163.
- (42) Bischoff, T.; Wiktor, J.; Chen, W.; Pasquarello, A. Nonempirical hybrid Functionals for Band gaps of Inorganic Metal-halide Perovskites. *Phys. Rev. Mater.* **2019**, *3*, 123802.
- (43) Wang, H.; Tal, A.; Bischoff, T.; Gono, P.; Pasquarello, A. Accurate and Efficient Band-gap Predictions for Metal Halide Perovskites at Finite Temperature. *npj Comput. Mater.* **2022**, *8*, 237.
- (44) Wang, H.; Ouyang, R.; Chen, W.; Pasquarello, A. High-Quality Data Enabling Universality of Band Gap Descriptor and Discovery of Photovoltaic Perovskites. *J. Am. Chem. Soc.* **2024**, *146*, 17636–17645.
- (45) Zhang, M.; Cui, Z.; Wang, Y.; Jiang, H. Hybrid Functionals with System-dependent Parameters: Conceptual Foundations and Methodological Developments. *WIREs Comput. Mol. Sci.* **2020**, *10*.
- (46) Zacharias, M.; Volonakis, G.; Giustino, F.; Even, J. Anharmonic Electron-phonon Coupling in Ultrasoft and Locally Disordered Perovskites. *npj Comput. Mater.* **2023**, *9*, 153.

- (47) Zacharias, M.; Volonakis, G.; Giustino, F.; Even, J. Anharmonic lattice dynamics via the special displacement method. *Phys. Rev. B* **2023**, *108*, 035155.
- (48) Even, J.; Pedesseau, L.; Jancu, J.-M.; Katan, C. Importance of Spin–Orbit Coupling in Hybrid Organic/Inorganic Perovskites for Photovoltaic Applications. *The Journal of Physical Chemistry Letters* **2013**, *4*, 2999–3005.
- (49) Zhao, X.-G.; Dalpian, G. M.; Wang, Z.; Zunger, A. Polymorphous Nature of Cubic Halide Perovskites. *Phys. Rev. B* **2020**, *101*, 155137.
- (50) Liu, P.; Franchini, C.; Marsman, M.; Kresse, G. Assessing Model-dielectric-dependent Hybrid Functionals on the Antiferromagnetic Transition-metal Monoxides MnO, FeO, CoO, and NiO. *J. Phys.: Condens. Matter* **2019**, *32*, 015502.
- (51) Baroni, S.; de Gironcoli, S.; Dal Corso, A.; Giannozzi, P. Phonons and Related Crystal Properties from Density-Functional Perturbation Theory. *Rev. Mod. Phys.* **2001**, *73*, 515–562.
- (52) Resta, R. Theory of the Electric Polarization in Crystals. *Ferroelectrics* **1992**, *136*, 51–55.
- (53) Gajdoš, M.; Hummer, K.; Kresse, G.; Furthmüller, J.; Bechstedt, F. Linear Optical Properties in the Projector-augmented Wave Methodology. *Phys. Rev. B* **2006**, *73*, 045112.
- (54) Hansen, K. R.; Wong, C. Y.; McClure, C. E.; Romrell, B.; Flannery, L.; Powell, D.; Garden, K.; Berzansky, A.; Eggleston, M.; King, D. J. et al. Mechanistic Origins of Excitonic Properties in 2D Perovskites: Implications for Exciton Engineering. *Matter* **2023**, *6*, 3463–3482.
- (55) Silver, S.; Yin, J.; Li, H.; Brédas, J.-L.; Kahn, A. Characterization of the Valence and Conduction Band Levels of $n = 1$ 2D Perovskites: A Combined Experimental and Theoretical Investigation. *Adv. Energy Mater.* **2018**, *8*, 1703468.
- (56) Du, K.-z.; Tu, Q.; Zhang, X.; Han, Q.; Liu, J.; Zauscher, S.; Mitzi, D. B. Two-Dimensional

- Lead(II) Halide-Based Hybrid Perovskites Templated by Acene Alkylamines: Crystal Structures, Optical Properties, and Piezoelectricity. *Inorg. Chem.* **2017**, *56*, 9291–9302.
- (57) Tanaka, K.; Kondo, T. Bandgap and Exciton Binding Energies in Lead-iodide-based Natural Quantum-well Crystals. *Sci. Technol. Adv. Mater.* **2003**, *4*, 599–604.
- (58) Ishihara, T.; Takahashi, J.; Goto, T. Optical Properties due to Electronic Transitions in Two-dimensional Semiconductors $(C_nH_{2n+1}NH_3)_2PbI_4$. *Phys. Rev. B* **1990**, *42*, 11099–11107.
- (59) Saponi, D.; Kepenekian, M.; Pedesseau, L.; Katan, C.; Even, J. Quantum Confinement and Dielectric Profiles of Colloidal Nanoplatelets of Halide Inorganic and Hybrid Organic–inorganic Perovskites. *Nanoscale* **2016**, *8*, 6369–6378.
- (60) Traore, B.; Pedesseau, L.; Assam, L.; Che, X.; Blancon, J.-C.; Tsai, H.; Nie, W.; Stoumpos, C. C.; Kanatzidis, M. G.; Tretiak, S. et al. Composite Nature of Layered Hybrid Perovskites: Assessment on Quantum and Dielectric Confinements and Band Alignment. *ACS Nano* **2018**, *12*, 3321–3332.
- (61) Sio, W. H.; Giustino, F. Unified ab initio Description of Fröhlich Electron-phonon Interactions in Two-dimensional and Three-dimensional materials. *Phys. Rev. B* **2022**, *105*, 115414.
- (62) Knutson, J. L.; Martin, J. D.; Mitzi, D. B. Tuning the Band Gap in Hybrid Tin Iodide Perovskite Semiconductors Using Structural Templating. *Inorg. Chem.* **2005**, *44*, 4699–4705.
- (63) Zhong, X.; Ni, X.; Sidhik, S.; Li, H.; Mohite, A. D.; Brédas, J.-L.; Kahn, A. Direct Characterization of Type-I Band Alignment in 2D Ruddlesden–Popper Perovskites. *Adv. Energy Mater.* **2022**, *12*, 2202333.
- (64) Sutton, R. J.; Filip, M. R.; Haghighirad, A. A.; Sakai, N.; Wenger, B.; Giustino, F.; Snaith, H. J. Cubic or Orthorhombic? Revealing the Crystal Structure of Metastable Black-Phase CsPbI₃ by Theory and Experiment. *ACS Energy Lett.* **2018**, *3*, 1787–1794.

- (65) Stoumpos, C. C.; Cao, D. H.; Clark, D. J.; Young, J.; Rondinelli, J. M.; Jang, J. I.; Hupp, J. T.; Kanatzidis, M. G. Ruddlesden–Popper Hybrid Lead Iodide Perovskite 2D Homologous Semiconductors. *Chem. Mater.* **2016**, 28, 2852–2867.